REVIEW

# Optimization of multi-color laser waveform for high-order harmonic generation*

Cheng Jin(金成)[1,†] and C D Lin(林启东)[2]

[1] Department of Applied Physics, Nanjing University of Science and Technology, Nanjing 210094, China
[2] J. R. Macdonald Laboratory, Department of Physics, Kansas State University, Manhattan 66506, USA

(Received 3 April 2016; revised manuscript received 29 April 2016; published online 20 July 2016)

With the development of laser technologies, multi-color light-field synthesis with complete amplitude and phase control would make it possible to generate arbitrary optical waveforms. A practical optimization algorithm is needed to generate such a waveform in order to control strong-field processes. We review some recent theoretical works of the optimization of amplitudes and phases of multi-color lasers to modify the single-atom high-order harmonic generation based on genetic algorithm. By choosing different fitness criteria, we demonstrate that: (i) harmonic yields can be enhanced by 10 to 100 times, (ii) harmonic cutoff energy can be substantially extended, (iii) specific harmonic orders can be selectively enhanced, and (iv) single attosecond pulses can be efficiently generated. The possibility of optimizing macroscopic conditions for the improved phase matching and low divergence of high harmonics is also discussed. The waveform control and optimization are expected to be new drivers for the next wave of breakthrough in the strong-field physics in the coming years.

**Keywords:** high-order harmonic generation, waveform optimization, genetic algorithm, single-attosecond pulse

**PACS:** 42.65.Ky, 42.65.Re, 31.70.Hq, 32.90.+a **DOI:** 10.1088/1674-1056/25/9/094213

## 1. Introduction

When an atomic or molecular gas medium is exposed to an intense laser pulse, an extreme nonlinear process occurs that leads to the generation of high harmonics of laser light, up to hundreds or thousands of order.[1–3] These harmonics offer the potential of becoming useful bright, coherent tabletop light sources from the extreme ultraviolet (XUV) to X-rays, either in the form of single attosecond pulses (SAPs) with the duration below about 100 as,[4,5] or in the form of attosecond pulse trains (APTs).[6] The progress in high-order harmonic generation (HHG) has already provided the essential tools to study time-resolved processes taking place on the attosecond timescale, thus opening a new field of attosecond science.[7] Another important application is HHG spectroscopy, by which atomic and molecular structure information can be retrieved from the measured high harmonic spectra.[8–11] For a dynamic molecular system, HHG may be used to probe structural evolution on the sub-femtosecond timescale.[12,13]

High harmonics are generated from all atoms in the gas medium coherently. They depend on the nonlinear macroscopic propagation of the fundamental laser beam together with the high-harmonic field. A full description of experimentally observed HHG spectra consists of two parts: (i) the single-atom response; that is, the induced dipole by the driving field, obtained by solving the time-dependent Schrödinger equation (TDSE) or equivalents; and (ii) the macroscopic response, through solving the three dimensional Maxwell's equations of the fundamental laser and the high-harmonic fields.[14–20] The single-atom response has been understood qualitatively in terms of the well-known three-step model proposed by Corkum and others.[21,22] First, an electron tunnels through a barrier formed by the combined atomic and laser fields at a certain time; second, it is accelerated in the laser field; and finally, as the laser reverses its direction, the electron is driven back to recombine with the ion, emitting high-energy photons. The highest energy of the HHG photon is given by $\hbar\omega = I_p + 3.17U_p$, where $U_p$ is the ponderomotive energy of a free electron in the laser field, $I_p$ is the ionization energy of the target gas, and $\hbar$ is the reduced Planck's constant. For a laser with intensity $I_L$ and wavelength $\lambda_L$, $U_p \propto I_L\lambda_L^2$. With femtosecond mid-infrared lasers operating at wavelengths of a few microns,[23,24] the cutoff energy $\hbar\omega$ can easily reach the X-ray region.[25] In comparison, HHG light has been limited to the extreme ultraviolet ($\sim$ 100 eV) if it is generated by the widely available Ti:sapphire lasers with a wavelength of around 0.8 μm.[26–29] An efficient buildup of macroscopic harmonic field requires favorable phase-matching conditions from all elementary induced dipoles,[30–32] which in turn depends on both the laser and gas target properties, such as laser intensity, laser focusing position, gas pressure, and so on.

One of the feasible ways to modify single-atom HHG re-

*Project supported by the Fundamental Research Funds for the Central Universities of China (Grant No. 30916011207), Chemical Sciences, Geosciences and Biosciences Division, Office of Basic Energy Sciences, Office of Science, U. S. Department of Energy (Grant No. DE-FG02-86ER13491), and Air Force Office of Scientific Research, USA (Grant No. FA9550-14-1-0255).

†Corresponding author. E-mail: cjin@njust.edu.cn

 

sponse is to alter the driving electric field at the sub-cycle level such that ionization and propagation in the laser field can be controlled. Enhancing the high harmonic yields is one of the major goals in many experimental and theoretical efforts. By using an 800-nm laser with its third harmonic where the half-cycle symmetry is maintained, Watanabe *et al.*[33] in a pioneering experiment showed the enhancement of up to a factor of ten for high harmonics in Ar in 1994. Since then two-color control has been widely applied in the measurements for enhancing the harmonic yield.[34,35] In the meanwhile, many theoretical simulations also have predicted the enhancement of the HHG.[36–44] Furthermore, the plateau harmonic yield in the two-color field has been found to scale as $\lambda^{-3}$–$\lambda^{-4}$[45] in comparison with the well-known wavelength scaling law of $\lambda^{-5}$–$\lambda^{-6}$ for the single-color field.[46–50] On the other hand, many theoretical works have discussed the extension of harmonic cutoff energies[51–56] and the generation of continuum harmonic spectra for the SAP[57–61] by combining two- or three-color laser fields. For example, in 2007, Zeng *et al.*[62] theoretically investigated the generation of ultrabroad XUV supercontinuum with a 148-eV spectral width in a two-color laser field by optimizing the phase delay, which can support an isolated 65-as pulse without the phase compensation. This work has aroused great theoretical interest for designing all kinds of multi-color laser combinations to produce the SAP or supercontinuum HHG spectra,[63–75] including APT-assisted ionization schemes via single photon absorption.[76–78]

Recently, with the advancement of optical parametric amplification (OPA) and optical parametric chirped-pulse amplification (OPCPA) technology, multi-color light-field synthesizer has enabled coherent wavelength multiplexing of ultrabroadband (over two or more octaves) pulses with full phase and amplitude control, thus allowing the generation of arbitrary optical waveforms.[79–92] This ability promises unique possibilities for high-degree control of the strong-field processes. (For reviews of experimental progress, see Refs. [93] and [94].) From the practical point of view, however, in a multi-color synthesizer one needs to consider a large number of degrees of freedom. To form an optical driver pulse by combining two, three, or even more interferometer spectral channels (or colors), the amplitudes, carrier-envelope phases (CEPs), and the relative time delays are all independently adjustable. To scan this parameter space experimentally is impractical. Instead, it is of critical importance to develop a robust optimal algorithm for fine-tuning the optical waveform for the HHG process. Some groups have developed such algorithm for different purposes using genetic algorithm[95–100] or using the optimal-control theory.[101–105]

In this review, we will focus on the genetic optimization of the single-atom HHG for enhancing the high-harmonic yield,[97,98,100] extending the cutoff energy,[95] generating the SAP,[96] and selectively enhancing given harmonics.[99] Optimization of the macroscopic HHG[106] will also be discussed. This article is organized as follows. In Section 2 we will present essential theoretical ingredients to carry out the genetic optimization. In Section 3 we will review the different optimization schemes for modifying the single-atom HHG by using multi-color laser pulses. In Section 4 we will address the optimization of macroscopic conditions for phase-matched harmonics at different geometries, such as the hollow waveguide, gas cell, and gas jet. Finally, a summary and outlook will be given in Section 5.

## 2. Theoretical methods

### 2.1. Waveform synthesis

A waveform is synthesized by coherently combining multiple single-color sinusoidal near-infrared or mid-infrared laser pulses. For example, combining three such linearly polarized pulses with the same polarization direction will give a new electric field

$$\begin{aligned} E(t) &= A_1(t)E_1\cos(\omega_1 t+\phi_1)+A_2(t)E_2\cos(\omega_2 t+\phi_2) \\ &\quad +A_3(t)E_3\cos(\omega_3 t+\phi_3), \end{aligned} \tag{1}$$

where each pulse is characterized by its temporal envelope $A_i(t)$, amplitude $E_i$, angular frequency $\omega_i$, and relative phase $\phi_i$. The CEP and the phase caused by the time delay between two pulses are all included in $\phi_i$. Temporal envelope $A_i$ is usually assumed the same for each color component, which could be a multi-cycle gaussian or cosine-squared envelope, or a single-cycle flat-top envelope with half-cycle ramps when the pulse is switched "on" and "off". In the optimization, the search goal is to modify the single-atom HHG process according to different purposes. The search parameter space of $\{E_1,E_2,E_3,\omega_1,\omega_2,\omega_3,\phi_1,\phi_2,\phi_3\}$ can be reduced by fixing some of these parameters. Eq. (1) can be easily generalized to multi-color lasers that have different polarization directions or are chirped.

### 2.2. Strong-field approximation and quantitative rescattering model

The strong field approximation (SFA) formulated by Lewenstein *et al.*[107] (see its extension for the HHG with mid-infrared lasers in Ref. [108]) is an efficient method to calculate the single-atom HHG response, in which the induced dipole moment in the time domain is

$$\begin{aligned} D(t) &= \mathrm{i}\int_{-\infty}^{\infty}\mathrm{d}\tau\left(\frac{\pi}{\varepsilon+\mathrm{i}\tau/2}\right)^{3/2} d^*[p_{\mathrm{st}}(t,\tau)+A(t)]g^*(t) \\ &\quad \times \mathrm{e}^{-\mathrm{i}S_{\mathrm{st}}(t,\tau)}d[p_{\mathrm{st}}(t,\tau)+A(t-\tau)] \\ &\quad \times E(t-\tau)g(t-\tau)+\mathrm{c.c.}, \end{aligned} \tag{2}$$

where $E(t)$ is the laser's electric field, $A(t)$ is the vector potential, $\varepsilon$ is a positive regularization constant, $p_{\mathrm{st}}$ and $S_{\mathrm{st}}$ are the stationary values of the momentum and the quasiclassical action, respectively. In Eq. (2), $g(t)=\exp[-\frac{1}{2}\int_{-\infty}^{t}\gamma(\tau)\mathrm{d}\tau]$ is

the ground state amplitude with the ionization rate $\gamma(\tau)$, and $d(t)$ is the field-free dipole transition matrix element between the ground state and the continuum state. The stationary value of the momentum is given by

$$p_{\rm st}(t,\tau) = -\frac{1}{\tau}\int_{t-\tau}^{t} {\rm d}t'' A(t''), \tag{3}$$

and the corresponding stationary action is

$$S_{\rm st}(t,\tau) = \int_{t-\tau}^{t} {\rm d}t'' \{\frac{1}{2}[p_{\rm st}+A(t'')]^2 + I_{\rm p}\}. \tag{4}$$

The quantitative rescattering (QRS) model,[109,110] as a semi-empirical method, extending and modifying the SFA, which relies on the approximate factorization of the HHG induced dipole, has been "justified" based on the numerical solution of the TDSE for atoms[111] and molecular ion $H_2^+$,[112] and has also been tested for a two-color laser field.[113] Taking an atomic target as an example, according to the QRS model, the induced dipole moment (complex and in the frequency domain) in a linearly polarized laser can be written as

$$D(\omega) = W(\omega)d(\omega), \tag{5}$$

where $W(\omega)$ is the returning electron wave packet and $d(\omega)$ is the laser-free photorecombination transition dipole of the atom. $|W(\omega)|^2$ describes the flux of the returning electrons and is the property of the laser itself. The optimization of linearly polarized multi-color laser pulses only modifies the returning electron wave packet without affecting the recombination dipole in the harmonic generation.

For a multi-color laser waveform composed of orthogonal linearly polarized waves, the SFA formulation of Eq. (2) can be straightforwardly written in two orthogonal polarization directions.[114] So far the QRS model has been applied to linearly polarized lights only.

### 2.3. Genetic algorithm

Genetic algorithm (GA)[115–117] as one of the evolutionary algorithms has been widely used in the search and optimization in a multi-parameter space. It also has been applied to study strong-field phenomena, such as retrieving atomic potentials using elastic differential cross sections between free electrons and atomic ions,[118] coherently controlling induced-dipole emission by optimizing laser-pulse amplitude and phase,[119] maximizing pulse energy and minimizing temporal coherence of XUV radiation by optimizing laser beam and nonlinear medium,[106] synthesizing SAP by optimizing short intense excitation laser pulses,[103] tailoring the temporal profile of laser pulse to identify separately the role of microscopic and macroscopic phenomena in the HHG,[120] studying specific harmonic order by formulating laser pulse in frequency domain,[105] and so on.

GA deals with highly nonlinear response functions, which would produce a predefined result after searching the parameter set. In GA, each candidate solution (called individual) can mutate and alter, and a population of candidate solutions evolves toward better ones. The evolution is an iterative process. The population in each iteration is defined as a generation. Here is how the algorithm works. It usually starts with a population of randomly generated individuals. Then the fitness of every individual is evaluated. The better fit individuals are selected from the current population. Their genomes are modified to form a new generation, which is then used in the next iteration. Note that the fitness is usually the value of the objective function in the optimization problem. The evolution process can be terminated if a satisfactory fitness level has been reached, or a maximum number of generations has been produced.

Before carrying out the GA, there are two essential problems: (i) choose an optimization parameter set; and (ii) determine a fitness function which is a real function using optimization parameters as variables plus additional constraints in the optimization process.

However, GA also has limitations. For instance, the evaluation of the fitness function for high-dimensional problems is very expensive, the termination criterion is varied in every problem since GA always gives the "better" solution in comparison to other solutions, and optimized solutions in the GA may converge to local optima rather than to the global optimum in many optimization problems. Such solutions are still acceptable for practical purposes once the optimization goal has been largely achieved. Alternative optimization algorithms may be applied to HHG optimization problems, such as new unconstrained optimization algorithm (NEWUOA)[121] and Broyden–Fletcher–Goldfarb–Shannon (BFGS) algorithm.[122]

## 3. Single-atom waveform optimization

In this section, we will review some examples of optimizing multi-color laser waveforms based on the GA. The principle and important results of the waveform optimization will be presented, which aims at modifying the single-atom HHG processes for the enhancement of high harmonic yields under different circumstances, the extension of the harmonic cutoff energy, the generation of the SAP, and the selection of the desired harmonic order.

### 3.1. Waveform synthesized by using two or three commensurate lasers

We start with a waveform synthesized by using two or three commensurate lasers, in which the wavelength of each color has been predetermined. The optimization is simplified by the need of considering only one optical cycle of the longest wavelength color in the waveform.[97,98]

### 3.1.1. Two-color combination: 1600 + 533 nm

For a two-color optimization, the wavelengths of the fundamental and the secondary lasers were chosen to be 1600 nm and 533 nm, respectively, and the CEP of the fundamental was set at $\phi_1 = 0$. The optimization parameter space consisted of $\{E_1, E_2, \phi_2\}$. The target atom was Ne. The optimization goal was to enhance the single-atom HHG over a broad energy region. Since ionization occurs in a very narrow time window in the tunnel ionization regime, the enhancement of one harmonic would automatically enhance a broad range of high harmonics. Thus the fitness function was set as the harmonic yield at the cutoff energy. Other constraints were also imposed: (i) the cutoff energy should be more or less maintained at the given value, which was obtained by using a reference single color of the 1600-nm laser with an intensity of $3 \times 10^{14}$ W/cm$^2$; (ii) the ionization level at the end of a single-cycle waveform should be less than a few percent; (iii) in the plateau region, high harmonics generated from "short"-trajectory electrons should be stronger than those from the "long" ones. The optimization was performed such that the total laser power for the single-color wave and the optimized wave were about the same. After optimization, the GA returned the peak intensity of $1.98 \times 10^{14}$ W/cm$^2$ for the 1600-nm laser and $1.32 \times 10^{14}$ W/cm$^2$ for the 533-nm laser, while the optimized phase $\phi_2 = 1.36\pi$.

Figure 1(a) depicts two waveforms over one optical cycle: the single-color sinusoidal wave of the fundamental (black) and the two-color synthesized field (red). For an electron returning with a kinetic energy of $2U_p$, the ionization time and recombination time for the "long"- (open circles) and "short"-trajectory electrons (solid circles) are indicated for each waveform. Here $U_p$ is defined with respect to the single-color sinusoidal wave. The inset gives the electric fields at ionization times versus the returning electron energies. Comparing the two waveforms, it is clear that: (i) the optimized wave has higher electric fields at the ionization times, thus leading to more returning electrons, and (ii) there are more "short"-trajectory electrons than "long" ones. Figures 1(b) and 1(c) show the temporal HHG emission by performing time-frequency wavelet analysis for the QRS-calculated spectrum. The strong enhancement of "short"-trajectory electrons and the smaller attochirp (steeper slope) for the optimized wave are clearly seen.

The one-cycle result in Fig. 1 has been applied to the realistic Gaussian laser pulses. With the optimized pulse, the calculated single-atom HHG spectra showed an enhancement of about two orders of magnitude over the single-color case. After macroscopic propagation calculations in a typical gas medium, the high harmonics in the plateau region were further enhanced, reflecting that there were more "short"-trajectory electrons contributing to the HHG.[97] These results demonstrated the successful strategy of including macroscopic propagation effects in the single-atom HHG optimization.

### 3.1.2. Three-color combinations: 1600 + 800, 533, and 400 nm

The same optimization procedure has been carried out for three-color synthesis, in which the fundamental laser was fixed at 1600 nm with $\phi_1 = 0$. The other two colors were chosen from 800, 533, or 400 nm. The optimization parameter space was enlarged to $\{E_1, E_2, E_3, \phi_2, \phi_3\}$. The optimized results have been shown in Ref. [97]. Since there were more parameters, the optimization tended to converge to local optima and returned with several different sets of laser parameters. They would result in nearly identical waveform and generate more or less identical HHG spectra. With the ionization level fixed, single-atom HHG yields from such three-color synthesized waveforms were only about two times higher than the previous two-color waveform.[97] The three-color waveform obviously would increase the difficulty in the laboratories, but it would provide more degrees of freedom for manipulating laser parameters.

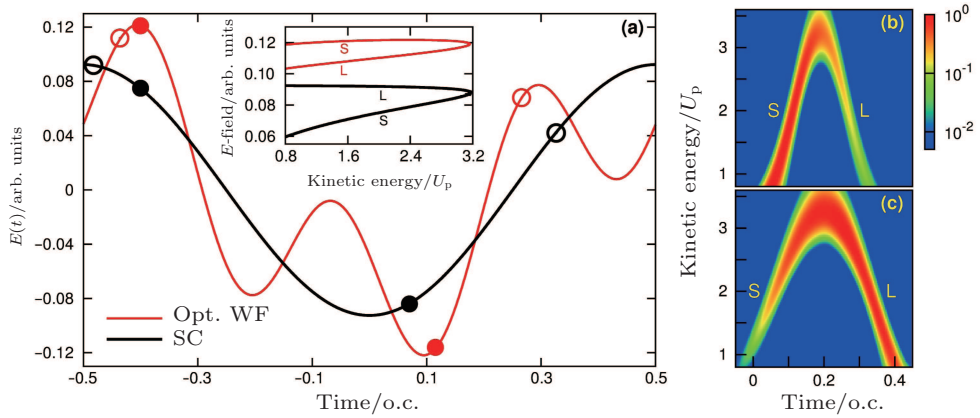


**Fig. 1.** (color online) (a) Comparison of a single-color (SC) sinusoidal wave and an optimized waveform (Opt. WF) over one optical cycle (o.c.) of the fundamental. Open and filled circles show the tunnel ionization and recombination times, for an electron with kinetic energy of $2U_p$ following the "long" or "short" trajectories, respectively. The inset depicts the electric fields at ionization time versus the kinetic energies of the returning electrons for "short"- and "long"-trajectory electrons, labeled as "S" and "L" in the figure, respectively. The yields of harmonic emission versus electron recombination times are shown for (b) the two-color and (c) the single-color waves, respectively. Adapted from Ref. [97].

### 3.2. Optimal mid-infrared wavelength in the two-color waveform

The development of mid-infrared laser technology has increased the central wavelength up to 7 μm,[24] which promises to greatly extend the HHG cutoff energy. However, harmonic yield drops very unfavorably with increasing laser wavelength.[46–50] Consider a specific question: what are the best mid-infrared wavelength and target atom for the generation of the highest harmonic yields for a given cutoff energy up to about 1 keV? An optimized two-color (the mid-infrared fundamental laser and its third harmonic) waveform has been identified in Section 3.1.1. So the optimization parameter space was $\{\lambda_1, E_1, E_2, \phi_2\}$, in which $\phi_1 = 0$ and $\lambda_2 = \lambda_1/3$, and the same optimization method in Section 3.1 was applied.[98]

In Ref. [98], for Ar, Ne, and He, the optimization has been carried out to search the shortest (also the optimal) fundamental wavelength $\lambda_1$ for the cutoff energy ranging from 0.2 to 1.0 keV. Compared to optimal single-color driving lasers, adding a third harmonic with a few percent intensity of the fundamental would give about the same given cutoff energy, but would generate much higher harmonic yields.[98]

We demonstrate the optimized results by taking one example with the cutoff energy at about 350 eV (the actual energy is 350 eV plus $I_p$ of the target). Single-atom HHG ($\propto \omega^4 |D(\omega)|^2$) spectra of the three targets calculated by the QRS model are shown in Fig. 2(a). The spectrum for Ne has the highest yields over a photon energy range of about 330 eV, followed by He, and then by Ar, when the total ionization probability is fixed at 2%. To understand these results, the HHG is separated into two parts in the spirit of the QRS model. The returning electron wave packets [defined as the modulus square of $W(\omega)$] for three targets are compared in Fig. 2(b), where He is a factor of two or three higher than Ne. However, as shown in Fig. 2(d), the photorecombination cross sections (PRCSs) for Ne are about ten times larger than He, thus ending up that Ne is more favorable for generating high harmonics up to the 350-eV region. The propagated results are shown in Fig. 2(c). The macroscopic conditions are: the laser beam waist $w_0$ for each color is 50 μm, 1-mm long gas jet is positioned at $z_R/2$ after the laser focus where the Rayleigh range of the fundamental laser is defined by $z_R = \pi w_0^2/\lambda_1$, and gas pressure of 10 Torr is uniformly distributed within the jet. From Fig. 2(c), macroscopic HHG spectrum from Ne is still the strongest one.

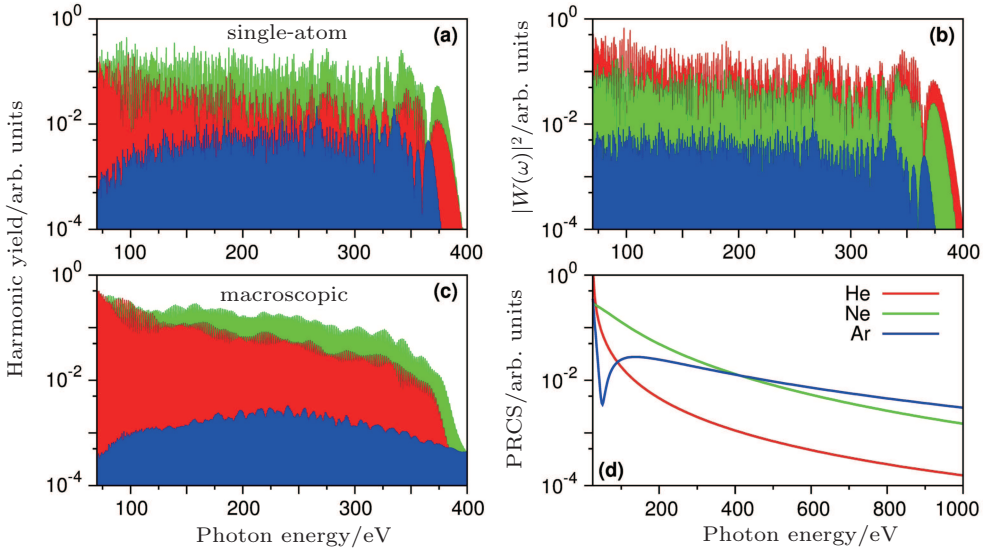


**Fig. 2.** (color online) (a) Single-atom and (c) macroscopic HHG spectra calculated by using the QRS model, and (b) returning electron wave packet calculated by the SFA. The maximum returning electron energy is fixed at 350 eV. The fundamental optimal wavelengths in the two-color waveforms are 2831, 1625 and 1350 nm for Ar, Ne and He, respectively. (d) Photorecombination cross sections (PRCSs) for the three targets over a broad photon energy region are shown. Adapted from Ref. [98].

### 3.3. Waveform synthesized by 800-nm and mid-infrared lasers

In Section 3.2, the two-color waveform consisting of a strong mid-infrared laser and a few percent of its third harmonic is able to extend the harmonic cutoff energy to the "water-window" and keV region with the optimal harmonic yield. To realize this scheme in the laboratories, one needs to wait for a high-power mid-infrared laser and a strong phase-controlled third harmonic. However, current wavelength-tunable, CEP-stabilized mid-infrared lasers are mostly pumped by 800-nm Ti:sapphire lasers, thus their pulse energies are smaller than pump lasers.[123,124] An alternative method is to synthesize an intense 800-nm Ti:sapphire laser with a relatively weaker long-wavelength mid-infrared laser. The wavelength of the latter was optimized, and it could be incommensurate with 800 nm and the optimization was performed over the whole laser pulse (the full-width-half-maximum or FWHM duration was assumed as 21.3 fs, eight optical cycles of the 800-nm laser) instead of a single cycle only as in Section 3.1 and Section 3.2. $\lambda_1$ was fixed at 800 nm,

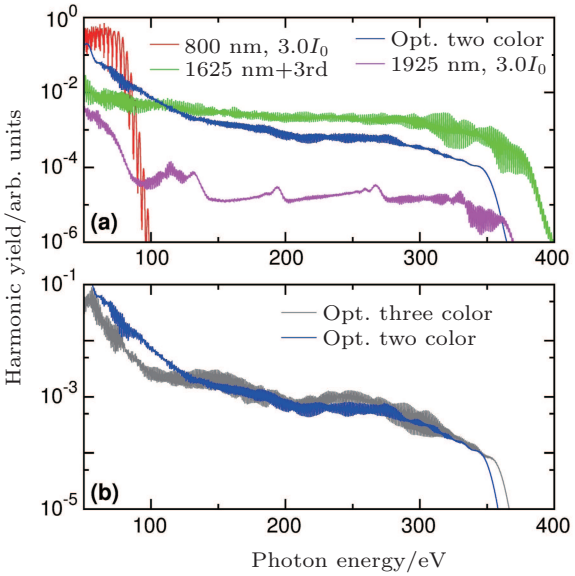


**Fig. 3.** (color online) Macroscopic HHG spectra of Ne calculated by the QRS model. (a) Two-color (800 + 2126 nm) waveform in the current scheme is compared with the two-color waveform (mid-infrared laser and its 3rd harmonic) in Fig. 2. One-color results are shown for reference. The parameters are indicated in the figures, $I_0$ is in the units of $10^{14}$ W/cm$^2$. (b) Comparison of the harmonic spectra by optimized two-(800 + 2126 nm) and three-color (800 + 2356 + 400 nm) waveforms. Adapted from Ref. [100].

$\phi_1 = 0$, and $E_1$ was larger than $E_2$. The search parameter space was $\{E_1, E_2, \lambda_2, \phi_2\}$. The optimization goal was to maximize the single-atom Ne HHG yield and to achieve the given cutoff energy with the ionization level of 4% over the whole pulse.[100]

The optimized laser parameters were obtained for the cutoff energy from 200 to 550 eV covering the "water-window" region: the peak intensity of the 800-nm laser was always about $2.0 \times 10^{14}$ W/cm$^2$, the wavelength and intensity of the mid-infrared laser increased monotonically with the increase of the cutoff energy, and the phase $\phi_2$ was quite stable. The macroscopic calculations were applied to test the single-atom optical waveform. The laser beam waist $w_0$ for each color was 50 μm, and the gas jet (1 mm long) was put at 2 mm after the focus. Gas pressure with uniform distribution in the jet was 10 Torr. For the cutoff energy of 350 eV, four different simulations with nearly identical total pulse energy are shown in Fig. 3(a). Clearly, a single 1925-nm laser can reach the required cutoff, but with the yield about 1000 times weaker than the 800-nm one. With the two-color waveform, by combining 800-nm and 2126-nm laser pulses, where the latter has about 50% of the energy of the former, the HHG yields over the same spectral range can be increased by about 30 to 100 times with the comparable total laser energy. The one with 1625 nm ($3.88 \times 10^{14}$ W/cm$^2$) plus its third harmonic gives the highest yields, however, they are only a factor of two or four larger than those in the current scheme, while the total power is slightly larger.

The three-color scheme has also been checked. With all other conditions staying more or less the same, a 400-nm laser was added as the third color, thus the search parameter space became $\{E_1, E_2, E_3, \lambda_2, \phi_2, \phi_3\}$. In Fig. 3(b), the macroscopic harmonic spectrum by optimally synthesizing 800-nm, 2356-nm, and 400-nm laser pulses is shown. Two-color (800 + 2126 nm) spectrum in Fig. 3(a) is also displayed for comparison. The two waveforms generate about the same harmonic yields, thus adding one more color does not help further enhancement of the harmonic yield.

### 3.4. "Perfect wave" to generate the maximum returning electron kinetic energy

According to the three-step model,[21,22] the maximum photon energy achieved in harmonic generation process is related to the maximum returning electron kinetic energy. The synthesis of multi-color laser pulses offers a potential way to extend the harmonic emission to high photon energies by shaping the waveform at the single-cycle level in which the electron motion in the laser field can be steered. Chipperfield *et al.*[95] have derived the so-called "perfect wave" for HHG, which generates returning electrons with the maximum possible energy for any given oscillation period $T$ and per period fluence $F$. This ideal waveform consists of a linear ramp with a dc offset, and is expressed as

$$E(t) = \pm\sqrt{\frac{F}{T}\frac{2}{\varepsilon_0 c}}\left(\frac{3t}{T} - 1\right), \tag{6}$$

for $0 \le t \le T$. In Eq. (6), $\varepsilon_0$ is the permittivity of free space and $c$ is the speed of light. In Fig. 4(a), the "perfect wave" is illustrated in the red line, and the trajectory of the electron with the maximum returning energy, starting at the ionization time $t_i = 0$ and ending up at the recombination time $t_r = T$, isshown in the green line. In this case, the maximum kinetic energy of the returning electron is about three times larger than that of a single-color sinusoidal field.

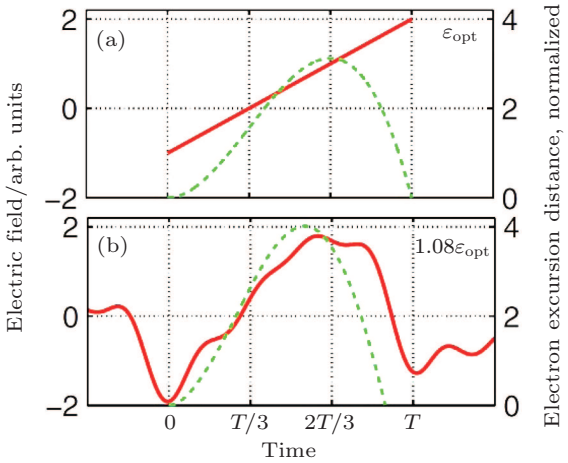


**Fig. 4.** (color online) The driving electric field (red lines) of (a) a "perfect wave" and (b) an optimized waveform consisting of the first four harmonics of $1/T$ and a field with a period of $2T$. Trajectories of the returning electrons with the maximum kinetic energies are also shown (green lines). $\varepsilon_{opt} = (e^2/m)(FT/4\varepsilon_0 c)$ is the maximum returning electron energy generated by the "perfect wave", where $e$ and $m$ are the electron charge and mass, respectively, $T$ is the oscillation period, and $F$ is per period fluence. Reprinted with permission from Ref. [95]. © (2009) by the American Physical Society.

In reality it is not possible to create the "perfect wave", because the generation of a linear ramp requires a large comb of frequencies and a high dc field is required for maintaining the asymmetric field amplitude. However, these can be ignored if one is only interested in generating a returning electron kinetic energy very close to the optimal value. A practically achievable approach has been proposed by Chipperfield *et al.*[95] to use the GA searching for the optimum waveform by coherently combining only a finite number of frequency components. In such optimization process, the fitness function was taken to be the returning electron kinetic energy, in which consideration of the electric field at the ionization time was also incorporated. The first four harmonics of $1/T$ and a field at half the fundamental frequency $1/2T$, limited to half the power of the fundamental, was used to obtain the optimized waveform. The search parameter space consisted of amplitudes and phases of five colors. The five-color optimal waveform is displayed in the red line of Fig. 4(b), which is capable of generating the returning electron energy as high as the "perfect wave". The calculations of high harmonics at typical macroscopic conditions have demonstrated that this optimized waveform retained the same harmonic yield as a pure sinusoidal pulse with the same periodicity.[95]

### 3.5. Waveform optimization for attosecond pulse generation

In 2011, Wirth *et al.*[85] reported the optical field synthesizer by dividing a white light super-continuum into three channels (spanning the infrared, visible, and ultraviolet frequency regimes, and covering 1.5 octaves) for the generation of sub-cycle laser pulses. Based on light field synthesis, Balogh *et al.*[96] have demonstrated in a recent theoretical work that attosecond pulse generation including the SAP generation could be controlled by optimally shaping the driver waveform. They added a fourth (UV) channel, together with three channels in Wirth *et al.*'s experimental spectra, to extend the total usable bandwidth to 1.88 octaves such that there are more freedom in the simulation. The optimization parameters in each channel included a time delay, the CEP, and the amplitude. SFA was applied to calculate the single-atom HHG response of Ne gas, and GA was used for the optimization. A fitness function was defined for different simulation goals, such as single shortest attosecond pulse generation or double-attosecond-pulse generation.

Here, only the waveform optimization for the SAP generation is discussed. Specifically, the fitness function was the shortest possible SAP with at least 10:1 contrast ratio by varying all free parameters. In the meanwhile, the integration time in the SFA calculation was limited to the short-time region such that harmonic emission from "long"-trajectory returning electrons can be eliminated. These integration times were obtained by classical calculations. After 50–80 generations, the GA was converged and returned the optimized parameters for generating a 55-as SAP. The corresponding laser field is shown in Fig. 5(a) including its electric field (solid black line) and the half-cycle period (red dashed line) defined as $\pi/|\mathrm{d}\varphi/\mathrm{d}t|$, where $\varphi$ is the phase of the laser field. The time-frequency analysis of the harmonic energies from 120 to 275 eV is presented in Fig. 5(b). The single-atom harmonic emission was calculated by the SFA, in which the integration time was not limited. The optimization determined that the best harmonic region for the shortest SAP production was 118- to 195-eV bandwidth, which gives a 55-as SAP in Fig. 5(c). If spectral filtering was used to select only "short" trajectory electrons,

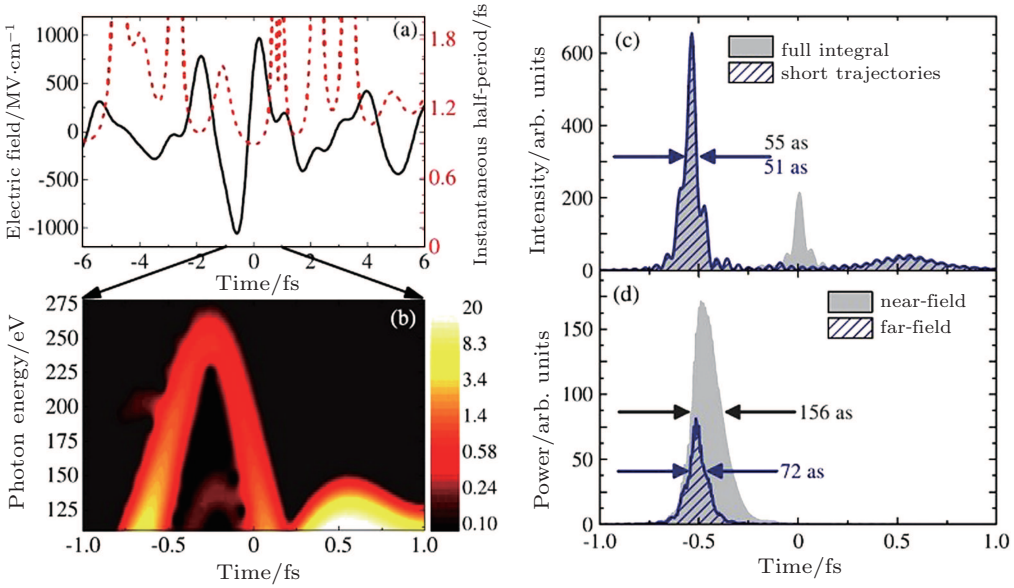


**Fig. 5.** (color online) (a) Electric field (black solid line) and instantaneous half-cycle period (red dashed line) of the optimized laser field. (b) The time-frequency picture of harmonic emission calculated by the full SFA. (c) Attosecond pulses by synthesizing single-atom harmonics between 118 and 195 eV. (d) Attosecond pulses generated after macroscopic propagation, in the near field and in the far field including small divergent ($< 1$ mrad) harmonic emissions only. Reprinted with permission from Ref. [96]. © (2014) by the American Physical Society.

the SAP duration was reduced to 51 as, and a second peak corresponding to "long" electron trajectories vanished as indicated in Fig. 5(c). Macroscopic calculations were performed to test the single-atom optimized generating field, which predicted a slightly longer 72-as pulse in Fig. 5(d) by filtering out harmonic emissions with the divergence angle $> 1$ mrad.

### 3.6. Waveform synthesis for selectively enhancing a few high harmonics

In 2013, Wei *et al.*[90] reported selective enhancement of a single harmonic by synthesizing an 800-nm laser and its second and third harmonics with perpendicular polarizations. The intensity contrast ratio between the target harmonic and adjacent harmonics was more than one order of magnitude. Other earlier studies have demonstrated similar enhancement of selective harmonics with quite different experimental scheme by shaping an 800-nm femtosecond pulse in the frequency domain.[119,125–127] A narrow frequency bandwidth around the central frequency was divided into dozens of small components and the phases of individual components were adjusted. Inspired by these works, Wang *et al.*[99] theoretically discussed the possibilities of combining the two techniques, i.e., pulse shaping and multi-color laser synthesizer, to achieve better harmonic control.

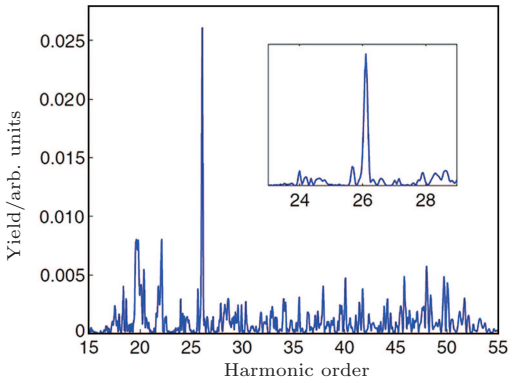


**Fig. 6.** (color online) Single-atom harmonic spectrum showing selectively enhancement of H26. The inset zooms in H26 with its nearest neighbors. A two-color field (800 + 267 nm) has been used with the optimized relative phase and chirp rates. Adapted from Ref. [99].

We will only review the simple case of two-color field combination with a linear chirp and the same polarization for both colors. Linear chirp rates of two colors and the relative phase between them were composed of the parameter search space. The fitness function was the yield of the highest harmonic peak with all other harmonics suppressed for a given fundamental intensity while the intensity ratio between the fundamental and its third harmonic was fixed.[99] One example of optimized single-atom harmonic spectra is shown in Fig. 6. The harmonic order 26 (H26) stands out prominently from the background. The inset zooms in H26 with its neighbor harmonics, and the contrast ratio between them is about ten times. In the simulation, the intensity of the fundamental 800-nm laser is $3.0 \times 10^{14}$ W/cm$^2$, the intensity ratio is 5%, and the FWHM duration of the laser pulse is ten optical cycles of the fundamental. Theoretical analysis indicated that for the chirp-optimized waveform, target harmonics emitted at different times (or optical cycles) have good temporal coherence, thus they add up constructively. The single-atom result has been tested by averaging harmonic spectra over a range of intensities to partially include macroscopic effects.[128] The enhancement of the target harmonic was maintained. It also has been shown that selectively enhancing two harmonic orders of interest was possible by a simple two-color-linear-chirp combination.[99]

## 4. Optimization of macroscopic conditions

In Section 3, we mostly focus on the optimization of the multi-color waveform at the single-atom response level. To realize such a waveform in the experiment or to achieve the ultimate goal of optimizing macroscopic high harmonics, we rely on the nonlinear propagation of both the driving laser and the high-harmonic fields in a macroscopic medium. The resulting harmonic yields are sensitive to macroscopic conditions, such as gas pressure, medium length, laser focusing position, laser beam size, and so on. Since each propagation calculation is already rather time consuming, it is not realistic to routinely optimize all the macroscopic parameters by simulations.

In this section, we will first review our recent work of optimizing a limited set of macroscopic parameters for a two-color waveform propagating in a hollow waveguide such that low-divergent soft x-ray high harmonics can be obtained.[129] We will then discuss possibilities of optimizing macroscopic parameters in other common HHG generation setups, such as a gas jet or a gas cell.

### 4.1. Waveform in a hollow waveguide

The hollow waveguide is a commonly used experimental setup for generating high harmonics, which has been implemented for creating quasi-phase matching (QPM) conditions,[130,131] selecting electron trajectory,[132] temporally and spatially shaping the driving laser pulse,[125,133] combining with a UV laser to efficiently producing soft X-ray harmonics,[134] and generating keV harmonics with mid-infrared lasers.[25,135,136] In a hollow waveguide, diffraction can be eliminated such that a spatially constant laser intensity can be maintained over an extended distance and the geometric phase does not depend on the radial distance. This is considered to be an ideal setup to keep a nearly constant waveform as the laser pulse propagates. We have proposed to combine two advanced technologies: multi-color laser synthesizer and laser guiding in the waveguide, to generate extremely bright high harmonics in the soft X-ray region. This goal has been achieved by optimizing the waveguide parameters (radius and length) and gas pressure.[129]

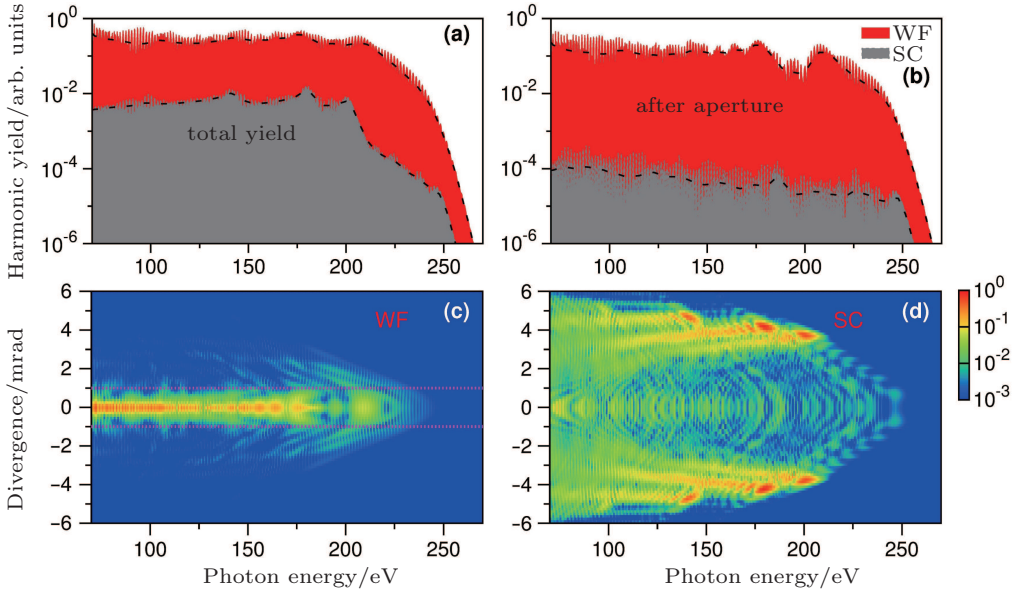


**Fig. 7.** (color online) (a) Total harmonic yield emitted at the exit of the hollow waveguide and (b) harmonic yield integrated within 1 mrad using an aperture in the far field for two-color (1.6+0.533 μm) waveform (WF) and single-color (SC) laser. The corresponding harmonic divergence in the far field for WF (c) and for SC (d). Length and radius of the waveguide are 5 mm and 125 μm, respectively, and gas pressure is 50 Torr. Adapted from Ref. [129].

Figure 7(a) shows the total harmonic yield (integrated over the exit plane of the hollow waveguide) generated by the two-color (1.6 + 0.555 μm) waveform at the optimal conditions (the radius and length of the waveguide are 125 μm and 5 mm, respectively, and the gas pressure is 50 Torr). These conditions ensure that the highest cutoff energy and the highest harmonic yields are achieved simultaneously. The two-color waveform used here has been optimized at the single-atom level favorable for the phase matching, as shown in Fig. 1(a). The harmonic yield from a reference 1.6-μm laser with the intensity of $3.0 \times 10^{14}$ W/cm$^2$ is also shown, which is about 1 to 2 orders of magnitude smaller than the two-color pulse. The harmonic emission in the far field for the two cases are shown in Figs. 7(c) and 7(d). Two-color high harmonics in the spectral range of 70 to 250 eV are well localized along the propagation axis with divergence angle smaller than 1 mrad. If one uses an aperture to filter out divergent harmonics (> 1 mrad), results in Fig. 7(b) show that two-color high harmonics have more than three orders of magnitude than the single-color ones. Further theoretical analysis uncovered that under the optimal waveguide parameters and gas pressure, the balance between waveguide mode, atomic dispersion, and plasma effect could be reached to achieve dynamic phase matching and the optimized two-color waveform was maintained throughout the hollow waveguide.[129]

This work demonstrates the advantage of a predetermined two-color laser waveform, such as enhancing the harmonic yield, suppressing the "long"-trajectory electron emission, maintaining the given cutoff energy, and minimizing the HHG phase-mismatch and laser defocusing, can be fully realized when macroscopic conditions are properly chosen. It also provides a scheme to limit the number of macroscopic parameters for the ultimate optimization.

### 4.2. Waveform in a gas jet or gas cell

A gas jet or gas cell is widely used in HHG experiments. A laser beam is usually focused to reach the required intensity to interact with a gas to initiate the HHG process. The distributions of intensity and phase of the laser beam are not uniform in space. By simply focusing multi-color laser beams into the same spot, the optimized waveform is maintained only in a very small spatial range. This method has been applied in the simulations in Section 3 to check macroscopic propagation effects for single-atom optimized waveforms.

Here we suggest two possible ways to optimize macroscopic conditions for a given multi-color laser waveform for the geometry of a gas jet or a gas cell. First, we assume the length of a gas cell is so short that the effects of nonuniform laser intensity and phase can be minimized and that defocusing of the laser beam is not serious. In this case, the gas pressure can be greatly increased and optimized to compensate the short gas-cell length. Second, for a typical 1–2 mm long gas jet, the combination of a multi-color laser beam can be optimized such that laser waveforms in the interaction region with the gas jet are the most closest to the given waveform. This involves adjustment of a large number of parameters, such as the gas-jet position, and the parameters determining laser focusing conditions and input energy for each color, and a proper definition of the best waveform referring to the given one. This is better accomplished by using an optimization algorithm, GA for example. Gas pressure can be treated as an additional free parameter. The macroscopic propagation calculations by solving the three-dimensional Maxwell's equations of the driving laser and high-harmonic fields should be used to check the out-

come of these approaches, thus modifying them accordingly.

## 5. Conclusions and perspective

We reviewed recent theoretical works of optimizing multi-color laser waveform for controlling single-atom HHG emission based on the GA. First, a waveform synthesized by two or three lasers with commensurate wavelengths was optimized together with partial optimization on macroscopic propagation effects. The results showed that harmonic yields could be enhanced by two orders of magnitude compared to a single-color field, without the increase of the laser power. Second, two-color waveforms with the shortest fundamental wavelength were proposed to optimally generate high harmonics with cutoff energies from 200 to 1000 eV for three common rare gases. Third, an intense 800-nm laser was suggested to be combined with a relatively weak and wavelength-tunable mid-infrared laser to generate harmonics with yields comparable to the previous two-color waveform in the "water-window" region. Then, the so-called "perfect wave" that generates the maximum possible returning electron energy over 3 times as high as that for a pure sinusoidal wave was discussed, which can be approached approximately by using a five-color laser optimal combinations. In addition, a four-color waveform synthesis was performed in an ultrabroad spectral range covering the ultraviolet-infrared domain for producing single or double attosecond pulses. Finally, multi-color synthesis of shaped single color pulses, which can be optimized to selectively generate one or two harmonic orders, was illustrated. We also discussed the possibilities of optimizing macroscopic conditions for different geometries. In a hollow waveguide, the two-color waveform optimized at the single-atom level was shown to be capable of generating intense soft-X-ray high harmonics with 1-mrad divergence by optimizing the waveguide parameters and gas pressure. The possible ways of optimizing macroscopic conditions for a gas jet or a gas cell were briefly addressed.

With the development of mid-infrared laser and multi-color synthesis technologies, waveform optimization will have a great and immediate impact on many research areas in strong-field physics. First, the emergence of hundreds kHz and MHz lasers,[27,137,138] combined with one or two orders enhancement of HHG yields from an optimized laser waveform, promises to increase photon number per second from the currently available ones by several orders, thus making HHG powerful tools for generating coherent tabletop light sources ranging from the extreme ultraviolet to X-rays in the laboratory. It can also be used to produce intense attosecond light pulses for attosecond-pump and attosecond-probe experiments for probing electron dynamics of atoms, molecules, and condensed materials at their intrinsic timescale. Second, optimized laser waveform can enhance the HHG signal without increasing laser power. Probing the structure or dynamics of molecules often requires the use of mid-infrared lasers to generate high energy returning electrons. Using lasers that have optimized waveforms can increase the flux of returning electrons without excessive ionization that depletes the target molecules. These increased electron fluxes would enhance many orders of magnitude of the HHG yields or high energy photoelectrons. The former allows one to use HHG spectroscopy to probe target molecules similar to photoionization experiments by a coherent broadband light source, for example, to study polyatomic molecules directly.[139] High energy photoelectron momentum spectra can be used for laser-induced electron diffraction (LIED), from which sub-angstrom spatial resolution of the interatomic distances can be retrieved.[140–142] Finally, laser waveform optimization provides more freedom to control and change the strong-field processes, such as THz generation,[143] laser-plasma interaction,[144] and particle acceleration. In short, theoretical efforts in waveform optimization and synthesis are expected to play a very important role in the coming years as experimentalists fine-tune their tools for complete control in the manipulation of laser's waveform for targeted goals. This topic is to become a major research area that will drive the next technological revolution in the strong-field physics and attosecond science.

## References


[1] Corkum P B and Krausz F 2007 *Nat. Phys.* **3** 381
[2] Agostini P and DiMauro L F 2004 *Rep. Prog. Phys.* **67** 813
[3] Chang Z, Rundquist A, Wang H, Murnane M M and Kapteyn H C 1997 *Phys. Rev. Lett.* **79** 2967
[4] Goulielmakis E, Schultze M, Hofstetter M, Yakovlev V S, Gagnon J, Uiberacker M, Aquila A L, Gullikson E M, Attwood D T, Kienberger R, Krausz F and Kleineberg U 2008 *Science* **320** 1614
[5] Zhao K, Zhang Q, Chini M, Wu Y, Wang X and Chang Z 2012 *Opt. Lett.* **37** 3891
[6] López-Martens R, Varjú K, Johnsson P, Mauritsson J, Mairesse Y, Salières P, Gaarde M B, Schafer K J, Persson A, Svanberg S, Wahlström C G and L'Huillier A 2005 *Phys. Rev. Lett.* **94** 033001
[7] Krausz F and Ivanov M 2009 *Rev. Mod. Phys.* **81** 163
[8] Itatani J, Levesque J, Zeidler D, Niikura H, Pépin H, Kieffer J C, Corkum P B and Villeneuve D M 2004 *Nature* **432** 867
[9] Haessler S, Caillat J, Boutu W, Giovanetti-Teixeira C, Ruchon T, Auguste T, Diveki Z, Breger P, Maquet A, Carré B, Taïeb R and Salières P 2010 *Nat. Phys.* **6** 200
[10] Vozzi C, Negro M, Calegari F, Sansone G, Nisoli M, De Silvestri S and Stagira S 2011 *Nat. Phys.* **7** 822
[11] Shiner A D, Schmidt B E, Trallero-Herrero C, Wörner H J, Patchkovskii S, Corkum P B , Kieffer J C, Légaré F and Villeneuve D M 2011 *Nat. Phys.* **7** 464
[12] Smirnova O, Mairesse Y, Patchkovskii S, Dudovich N, Villeneuve D, Corkum P and Ivanov M Y 2009 *Nature* **460** 972
[13] Wörner H J, Bertrand J B, Kartashov D V, Corkum P B and Villeneuve D M 2010 *Nature* **466** 604
[14] Gaarde M B, Tate J L and Schafer K J 2008 *J. Phys. B-At. Mol. Opt. Phys.* **41** 132001
[15] Jin C, Le A T and Lin C D 2011 *Phys. Rev. A* **83** 023411
[16] Jin C 2013 *Theory of Nonlinear Propagation of High Harmonics Generated in a Gaseous Medium* (Springer) pp. 34–41
[17] Takahashi E, Tosa V, Nabekawa Y and Midorikawa K 2003 *Phys. Rev. A* **68** 023808
[18] Geissler M, Tempea G, Scrinzi A, Schnürer M, Krausz F and Brabec T 1999 *Phys. Rev. Lett.* **83** 2930
[19] Rae S C and Burnett K 1992 *Phys. Rev. A* **46** 1084

[20] Priori E, Cerullo G, Nisoli M, Stagira S, De Silvestri S, Villoresi P, Poletto L, Ceccherini P, Altucci C, Bruzzese R and de Lisio C 2000 *Phys. Rev. A* **61** 063801
[21] Corkum P B 1993 *Phys. Rev. Lett.* **71** 1994
[22] Krause J L, Schafer K J and Kulander K C 1992 *Phys. Rev. Lett.* **68** 3535
[23] Hong K H, Lai C J, Siqueira J, Krogen P, Moses J, Chang C L, Stein G J, Zapata L E and Kärtner F X 2014 *Opt. Lett.* **39** 3145
[24] Sanchez D, Hemmer M, Baudisch M, Cousin S L, Zawilski K, Schunemann P, Chalus O, Simon-Boisson C and Biegert J 2016 *Optica* **3** 147
[25] Popmintchev T, Chen M C, Popmintchev D, Arpin P, Brown S, Ališauskas S, Andriukaitis G, Balčiunas T, Mücke O D, Pugzlys A, Baltuška A, Shim B, Schrauth S E, Gaeta A, Hernández-García C, Plaja L, Becker A, Jaron-Becker A, Murnane M M and Kapteyn H C 2012 *Science* **336** 1287
[26] Chini M, Wang X, Cheng Y, Wang H, Wu Y, Cunningham E, Li P C, Heslar J, Telnov D A, Chu S I and Chang Z 2014 *Nat. Photonics* **8** 437
[27] Pupeza I, Holzberger S, Eidam T, Carstens H, Esser D, Weitenberg J, Rußbüldt P, Rauschenberger J, Limpert J, Udem T, Tünnermann A, Hänsch T W, Apolonski A, Krausz F and Fill E 2013 *Nat. Photonics* **7** 608
[28] Dubrouil A, Hort O, Catoire F, Descamps D, Petit S, Mével E, Strelkov V V and Constant E 2014 *Nat. Commun.* **5** 4637
[29] Wang L F, He X K, Teng H, Yun C X, Zhang W and Wei Z Y 2014 *Acta Phys. Sin.* **63** 224103 (in Chinese)
[30] Constant E, Garzella D, Breger P, Mével E, Dorrer C, Le Blanc C, Salin F and Agostini P 1999 *Phys. Rev. Lett.* **82** 1668
[31] Kazamias S, Douillet D, Weihe F, Valentin C, Rousse A, Sebban S, Grillon G, Augé F, Hulin D and Balcou P 2003 *Phys. Rev. Lett.* **90** 193901
[32] Yakovlev V S, Ivanov M and Krausz F 2007 *Opt. Express* **15** 15351
[33] Watanabe S, Kondo K, Nabekawa Y, Sagisaka A and Kobayashi Y 1994 *Phys. Rev. Lett.* **73** 2692
[34] Kim I J, Kim C M, Kim H T, Lee G H, Lee Y S, Park J Y, Cho D J and Nam C H 2005 *Phys. Rev. Lett.* **94** 243901
[35] Brizuela F, Heyl C M, Rudawski P, Kroon D, Rading L, Dahlström J M, Mauritsson J, Johnsson P, Arnold C L and L'Huillier A 2013 *Sci. Rep.* **3** 1410
[36] Protopapas M, Sanpera A, Knight P L and Burnett K 1995 *Phys. Rev. A* **52** R2527
[37] Schiessl K, Persson E, Scrinzi A and Burgdörfer J 2006 *Phys. Rev. A* **74** 053412
[38] Kondo K, Kobayashi Y, Sagisaka A, Nabekawa Y and Watanabe S 1996 *J. Opt. Soc. Am. B* **13** 424
[39] Pi L W, Shi T Y and Qiao H X 2006 *Chin. Phys. Lett.* **23** 1490
[40] Zhai Z, Yu R F, Liu X S and Yang Y J 2008 *Phys. Rev. A* **78** 041402
[41] Zhang G T, Wu J, Xia C L and Liu X S 2009 *Phys. Rev. A* **80** 055404
[42] Li F, Wang G L, Zhao S F and Zhou X X 2015 *Chin. Phys. Lett.* **32** 014210
[43] Kohler M C and Hatsagortsyan K Z 2012 *Phys. Rev. A* **85** 023819
[44] Gaarde M B, Schafer K J, Heinrich A, Biegert J and Keller U 2005 *Phys. Rev. A* **72** 013411
[45] Lan P, Takahashi E J and Midorikawa K 2010 *Phys. Rev. A* **81** 061802
[46] Shiner A D, Trallero-Herrero C, Kajumba N, Bandulet H C, Comtois D, Légaré F, Giguère M, Kieffer J C, Corkum P B and Villeneuve D M 2009 *Phys. Rev. Lett.* **103** 073902
[47] Tate J, Auguste T, Muller H G, Salières P, Agostini P and DiMauro L F 2007 *Phys. Rev. Lett.* **98** 013901
[48] Schiessl K, Ishikawa K L, Persson E and Burgdörfer J 2007 *Phys. Rev. Lett.* **99** 253903
[49] Frolov M V, Manakov N L and Starace A F 2008 *Phys. Rev. Lett.* **100** 173001
[50] Le A T, Wei H, Jin C, Tuoc V N, Morishita T and Lin C D 2014 *Phys. Rev. Lett.* **113** 033001
[51] Ishikawa K 2003 *Phys. Rev. Lett.* **91** 043002
[52] Ivanov I A and Kheifets A S 2009 *Phys. Rev. A* **80** 023809
[53] Wang B, Li X and Fu P 2000 *Phys. Rev. A* **62** 063816
[54] Wu J, Zhang G T, Xia C L and Liu X S 2010 *Phys. Rev. A* **82** 013411
[55] Xu J, Zeng B and Yu Y 2010 *Phys. Rev. A* **82** 053822
[56] Zhao D and Li F L 2013 *Chin. Phys. B* **22** 064215
[57] Pfeife T, Gallmann L, Abel M J, Nagel P M, Neumark D M and Leone S R 2006 *Phys. Rev. Lett.* **97** 163901
[58] Kim C M and Nam C H 2006 *J. Phys. B-At. Mol. Opt. Phys.* **39** 3199
[59] Kim B, Ahn J, Yu Y, Cheng Y, Xu Z and Kim D E 2008 *Opt. Express* **16** 10331
[60] Tosa V, Altucci C, Kovács K, Negro M, Stagira S, Vozzi C and Velotta R 2012 *IEEE J. Sel. Top. Quant.* **18** 239
[61] Xia C L and Miao X Y 2015 *Chin. Phys. Lett.* **32** 043202
[62] Zeng Z, Cheng Y, Song X, Li R and Xu Z 2007 *Phys. Rev. Lett.* **98** 203901
[63] Li P C, Liu I L and Chu S I 2011 *Opt. Express* **19** 23857
[64] Du H, Wang H and Hu B 2010 *Phys. Rev. A* **81** 063813
[65] Du H and Hu B 2011 *Phys. Rev. A* **84** 023817
[66] Hong W, Lu P, Li Q and Zhang Q 2009 *Opt. Lett.* **34** 2102
[67] Lan P, Takahashi E J and Midorikawa K 2010 *Phys. Rev. A* **82** 053413
[68] Zhang X, Li Q, Yi X, Lv H and Ding Y 2013 *Opt. Commun.* **291** 285
[69] Zhang Q, He L, Lan P and Lu P 2014 *Opt. Express* **22** 13213
[70] Song X, Zeng Z, Fu Y, Cai B, Li R, Cheng Y and Xu Z 2007 *Phys. Rev. A* **76** 043830
[71] Zou P, Zeng Z, Zheng Y, Lu Y, Liu P, Li R and Xu Z 2010 *Phys. Rev. A* **81** 033428
[72] Feng L and Chu T 2011 *Phys. Rev. A* **84** 053853
[73] Lu R F, He H X, Guo Y H and Han K L 2009 *J. Phys. B-At. Mol. Opt. Phys.* **42** 225601
[74] Yu C, Wang Y, Cao X, Jiang S and Lu R 2014 *J. Phys. B-At. Mol. Opt. Phys.* **47** 225602
[75] Zhang C and Liu C 2015 *New J. Phys.* **17** 023026
[76] Zhao S F, Zhou X X, Li P C and Chen Z 2008 *Phys. Rev. A* **78** 063404
[77] Li P C, Zhou X X, Wang G L and Zhao Z X 2009 *Phys. Rev. A* **80** 053825
[78] Lan P, Lu P, Cao W and Wang X 2007 *Phys. Rev. A* **76** 043808
[79] Vozzi C, Calegari F, Frassetto F, Poletto L, Sansone G, Villoresi P, Nisoli M, De Silvestri S and Stagira S 2009 *Phys. Rev. A* **79** 033842
[80] Bandulet H C, Comtois D, Bisson E, Fleischer A, Pépin H, Kieffer J C, Corkum P B and Villeneuve D M 2010 *Phys. Rev. A* **81** 013803
[81] Siegel T, Torres R, Hoffmann D J, Brugnera L, Procino I, Zaïr A, Underwood J G, Springate E, Turcu I C E, Chipperfield L E and Marangos J P 2010 *Opt. Express* **18** 6853
[82] Oishi Y, Kaku M, Suda A, Kannari F and Midorikawa K 2006 *Opt. Express* **14** 7230
[83] Takahashi E J, Lan P, Mücke O D, Nabekawa Y and Midorikawa K 2010 *Phys. Rev. Lett.* **104** 233901
[84] Huang S W, Cirmi G, Moses J, Hong K H, Bhardwaj S, Birge J R, Chen L J, Li E, Eggleton B J, Cerullo G and Kärtner F X 2011 *Nat. Photonics* **5** 475
[85] Wirth A, Hassan M T, Grguraš I, Gagnon J, Moulet A, Luu T T, Pabst S, Santra R, Alahmed Z A, Azzeer A M, Yakovlev V S, Pervak V, Krausz F and Goulielmakis E 2011 *Science* **334** 195
[86] Takahashi E J, Lan P, Mücke O D, Nabekawa Y and Midorikawa K 2013 *Nat. Commun.* **4** 2691
[87] Haessler S, Balčiunas T, Fan G, Andriukaitis G, Pugžlys A, Baltuška A, Witting T, Squibb R, Zaïr A, Tisch J W G, Marangos J P and Chipperfield L E 2014 *Phys. Rev. X* **4** 021028
[88] Ishii N, Kosuge A, Hayashi T, Kanai T, Itatani J, Adachi S and Watanabe S 2008 *Opt. Express* **16** 20876
[89] Dao L V, Dinh K B and Hannaford P 2015 *Nat. Commun.* **6** 7175
[90] Wei P, Miao J, Zeng Z, Li C, Ge X, Li R and Xu Z 2013 *Phys. Rev. Lett.* **110** 233903
[91] Wei P, Zeng Z, Jiang J, Miao J, Zheng Y, Ge X, Li C and Li R 2014 *Appl. Phys. Lett.* **104** 151101
[92] Schütt B, Weber P, Kovács K, Balogh E, Major B, Tosa V, Han S, Vrakking M J J, Varjú K and Rouzée A 2015 *Opt. Express* **23** 33947
[93] Manzoni C, Mücke O D, Cirmi G, Fang S, Moses J, Huang S W, Hong K H, Cerullo G and Kärtner F X 2015 *Laser Photonics Rev.* **9** 129
[94] Mücke O D, Fang S, Cirmi G, Rossi G M, Chia S H, Ye H, Yang Y, Mainz R, Manzoni C, Farinello P, Cerullo G and Kärtner F X 2015 *IEEE J. Sel. Top. Quant.* **22** 1
[95] Chipperfield L E, Robinson J S, Tisch J W G and Marangos J P 2009 *Phys. Rev. Lett.* **102** 063003
[96] Balogh E, Bódi B, Tosa V, Goulielmakis E, Varjú K and Dombi P 2014 *Phys. Rev. A* **90** 023855
[97] Jin C, Wang G, Wei H, Le A T and Lin C D 2014 *Nat. Commun.* **5** 4003
[98] Jin C, Wang G, Le A T and Lin C D 2014 *Sci. Rep.* **4** 7067
[99] Wang X, Jin C and Lin C D 2014 *Phys. Rev. A* **90** 023416

[100] Jin C, Hong K H and Lin C D 2015 *Opt. Lett.* **40** 3754

[101] Chou Y, Li P C, Ho T S and Chu S I 2015 *Phys. Rev. A* **91** 063408

[102] Solanpää J, Budagosky J A, Shvetsov-Shilovski N I, Castro A, Rubio A and Räsänen E 2014 *Phys. Rev. A* **90** 053402

[103] Ben Haj Yedder A, Le Bris C, Atabek O, Chelkowski S and Bandrauk A D 2004 *Phys. Rev. A* **69** 041802

[104] Hellgren M, Räsänen E and Gross E K U 2013 *Phys. Rev. A* **88** 013414

[105] Schaefer I and Kosloff R 2012 *Phys. Rev. A* **86** 063417

[106] Roos L, Gaarde M B and L'Huillier A 2001 *J. Phys. B-At. Mol. Opt. Phys.* **34** 5041

[107] Lewenstein M, Balcou P, Ivanov M Y, L'Huillier A and Corkum P B 1994 *Phys. Rev. A* **49** 2117

[108] Le A T, Wei H, Jin C and Lin C D 2016 *J. Phys. B-At. Mol. Opt. Phys.* **49** 053001

[109] Morishita T, Le A T, Chen Z and Lin C D 2008 *Phys. Rev. Lett.* **100** 013903

[110] Le A T, Lucchese R R, Tonzani S, Morishita T and Lin C D 2009 *Phys. Rev. A* **80** 013401

[111] Le A T, Morishita T and Lin C D 2008 *Phys. Rev. A* **78** 023814

[112] Le A T, Picca R D, Fainstein P D, Telnov D A, Lein M and Lin C D 2008 *J. Phys. B-At. Mol. Opt. Phys.* **41** 081002

[113] Zhao S F, Wang Y, Wang G and Zhou X X 2014 *Opt. Commun.* **328** 30

[114] Antoine P, L'Huillier A, Lewenstein M, Salière P and Carré B 1996 *Phys. Rev. A* **53** 1725

[115] Carroll D L 2001 *FORTRAN Genetic Algorithm Driver*, version 1.7a

[116] Goldberg D E 1989 *Genetic Algorithms in Search, Optimization and Machine Learning* (Reading: Addison-Wesley Professional)

[117] Mitchell M 1996 *An Introduction to Genetic Algorithms* (Cambridge: MIT Press)

[118] Xu J, Zhou H L, Chen Z and Lin C D 2009 *Phys. Rev. A* **79** 052508

[119] Chu X and Chu S I 2001 *Phys. Rev. A* **64** 021403

[120] Boyko O, Valentin C, Mercier B, Coquelet C, Pascal V, Papalazarou E, Rey G and Balcou P 2007 *Phys. Rev. A* **76** 063811

[121] Powell M J D 2008 *IMA J. Numer. Anal.* **28** 649

[122] Fletcher R 2000 *Practical Methods of Optimization*, 2nd edn. (New York: Wiley)

[123] Ishii N, Kaneshima K, Kitano K, Kanai T, Watanabe S and Itatani J 2014 *Nat. Commun.* **5** 3331

[124] Cousin S L, Silva F, Teichmann S, Hemmer M, Buades B and Biegert J 2014 *Opt. Lett.* **39** 5383

[125] Bartels R, Backus S, Zeek E, Misoguti L, Vdovin G, Christov I P, Murnane M M and Kapteyn H 2000 *Nature* **406** 164

[126] Reitze D H, Kazamias S, Weihe F, Mullot G, Douillet D, Augé F, Albert O, Ramanathan V, Chambaret J P, Hulin D and Balcou P 2004 *Opt. Lett.* **29** 86

[127] Walter D, Pfeiffer T, Winterfeldt C, Kemmer R, Spitzenpfeil R, Gerber G and Spielmann C 2006 *Opt. Express* **14** 3433

[128] Jin C, Le A T and Lin C D 2009 *Phys. Rev. A* **79** 053413

[129] Jin C, Stein G J, Hong K H and Lin C D 2015 *Phys. Rev. Lett.* **115** 043901

[130] Gibson E A, Paul A, Wagner N, Tobey R, Gaudiosi D, Backus S, Christov I P, Aquila A, Gullikson E M, Attwood D T, Murnane M M and Kapteyn H C 2003 *Science* **302** 95

[131] Zhang X, Lytle A L, Popmintchev T, Zhou X, Kapteyn H C, Murnane M M and Cohen O 2007 *Nat. Phys.* **3** 270

[132] Igarashi H, Makida A and Sekikawa T 2013 *Opt. Express* **21** 20632

[133] Winterfeldt C, Spielmann C and Gerber G 2008 *Rev. Mod. Phys.* **80** 117

[134] Popmintchev D, Hernández-García C, Dollar F, *et al.* 2015 *Science* **350** 1225

[135] Popmintchev T, Chen M C, Bahabad A, Gerrity M, Sidorenko P, Cohen O, Christov I P, Murnane M M and Kapteyn H C 2009 *Proc. Natl. Acad. Sci. USA* **106** 10516

[136] Chen M C, Arpin P, Popmintchev T, Gerrity M, Zhang B, Seaberg M, Popmintchev D, Murnane M M and Kapteyn H C 2010 *Phys. Rev. Lett.* **105** 173901

[137] Krebs M, Hädrich S, Demmler S, Rothhardt J, Zaïr A, Chipperfield L, Limpert J and Tünnermann A 2013 *Nat. Photonics* **7** 555

[138] Hädrich S, Krebs M, Hoffmann A, Klenke A, Rothhardt J, Limpert J and Tünnermann A 2015 *Light-Sci. Appl.* **4** e320

[139] Wong M C H, Le A T, Alharbi A F, Boguslavskiy A E, Lucchese R R, Brichta J P, Lin C D and Bhardwaj V R 2013 *Phys. Rev. Lett.* **110** 033006

[140] Blaga C I, Xu J, DiChiara A D, Sistrunk E, Zhang K, Agostini P, Miller T A, DiMauro L F and Lin C D 2012 *Nature* **483** 194

[141] Xu J, Blaga C I, Zhang K, Lai Y H, Lin C D, Miller T A, Agostini P and DiMauro L F 2014 *Nat. Commun.* **5** 4635

[142] Pullen M G, Wolter B, Le A T, Baudisch M, Hemmer M, Senftleben A, Schröter C D, Ullrich J, Moshammer R, Lin C D and Biegert J 2015 *Nat. Commun.* **6** 7262

[143] Clerici M, Peccianti M, Schmidt B E, Caspani L, Shalaby M, Giguère M, Lotti A, Couairon A, Légaré F, Ozaki T, Faccio D and Morandotti R 2013 *Phys. Rev. Lett.* **110** 253901

[144] Heissler P, Hörlein R, Mikhailova J M, Waldecker L, Tzallas P, Buck A, Schmid K, Sears C M S, Krausz F, Veisz L, Zepf M and Tsakiris G D 2012 *Phys. Rev. Lett.* **108** 235003